AGU PUBLICATIONS

JGR

Journal of Geophysical Research: Oceans

RESEARCH ARTICLE

10.1002/2016JC011687

Large flux of iron from the Amery Ice Shelf marine ice to Prydz Bay, East Antarctica

L. Herraiz-Borreguero[1,2], D. Lannuzel[3,4], P. van der Merwe[3], A. Treverrow[3], and J. B. Pedro[1]

[1]Centre for Ice and Climate, Niels Bohr Institute, University of Copenhagen, Copenhagen, Denmark, [2]Now at National Oceanographic Center, University of Southampton, Southampton, UK, [3]Antarctic Climate and Ecosystems Cooperative Research Centre, University of Tasmania, Hobart, Tasmania, Australia, [4]Institute for Marine and Antarctic Studies, University of Tasmania, Hobart, Tasmania, Australia

Key Points:

- Marine ice provides a rich reservoir of bioavailable Fe, with implications for Antarctic marine productivity
- Melting marine ice can contribute to phytoplankton blooms in Prydz Bay, the third most productive bay in Antarctica
- Based on future rates of ice shelf basal melt, this fertilization pathway is likely to increase

Correspondence to:

L. Herraiz-Borreguero,
L.Herraiz-Borreguero@noc.soton.ac.uk

Citation:

Herraiz-Borreguero, L., D. Lannuzel, P. van der Merwe, A. Treverrow, and J. B. Pedro (2016), Large flux of iron from the Amery Ice Shelf marine ice to Prydz Bay, East Antarctica, *J. Geophys. Res. Oceans*, *121*, 6009–6020, doi:10.1002/2016JC011687.

Received 28 JAN 2016
Accepted 14 JUL 2016
Accepted article online
Published online 19 AUG 2016

Abstract The Antarctic continental shelf supports a high level of marine primary productivity and is a globally important carbon dioxide (CO_2) sink through the photosynthetic fixation of CO_2 via the biological pump. Sustaining such high productivity requires a large supply of the essential micronutrient iron (Fe); however, the pathways for Fe delivery to these zones vary spatially and temporally. Our study is the first to report a previously unquantified source of concentrated bioavailable Fe to Antarctic surface waters. We hypothesize that Fe derived from subglacial processes is delivered to euphotic waters through the accretion (Fe storage) and subsequent melting (Fe release) of a marine-accreted layer of ice at the base of the Amery Ice Shelf (AIS). Using satellite-derived Chlorophyll-a data, we show that the soluble Fe supplied by the melting of the marine ice layer is an order of magnitude larger than the required Fe necessary to sustain the large annual phytoplankton bloom in Prydz Bay. Our finding of high concentrations of Fe in AIS marine ice and recent data on increasing rates of ice shelf basal melt in many of Antarctica's ice shelves should encourage further research into glacial and marine sediment transport beneath ice shelves and their sensitivity to current changes in basal melt. Currently, the distribution, volume, and Fe concentration of Antarctic marine ice is poorly constrained. This uncertainty, combined with variable forecasts of increased rates of ice shelf basal melt, limits our ability to predict future Fe supply to Antarctic coastal waters.

1. Introduction

Across much of the Southern Ocean, primary production is low as a result of iron (Fe) limitation [*de Baar et al.*, 1990]. A prominent exception occurs in marine productivity "hot spots" around Antarctica, such as coastal polynyas, which are also globally important sinks for atmospheric carbon dioxide (CO_2) [*Arrigo and Van Dijken*, 2003; *Arrigo et al.*, 2015].

Various sources deliver Fe to the surface waters within the Southern Ocean: atmospheric dusts [*Jickells et al.*, 2005; *Fan et al.*, 2006], diapycnal diffusion [*Tagliabue et al.*, 2014], deep winter mixing [*Tagliabue et al.*, 2014], riverine discharge [*Raiswell and Canfield*, 2012], benthic recycling [*Raiswell and Canfield*, 2012], melting sea ice [*Lannuzel et al.*, 2007; *van der Merwe et al.*, 2009], and icebergs [*Raiswell et al.*, 2008; *Lin et al.*, 2011; *Smith et al.*, 2011]. More recently, subglacial meltwater has been postulated to naturally enrich surface waters with Fe and therefore fuel phytoplankton blooms up to 300 km away from the meltwater source [*Gerringa et al.*, 2012; *Alderkamp et al.*, 2012; *Death et al.*, 2014; *Hawkings et al.*, 2014; *van der Merwe et al.*, 2015]. Despite the growing interest in glacially-derived Fe input to surface waters, only limited Fe concentration and phase speciation data are available from the potential sources. The few measurements available are from meltwater runoff from the (more accessible) Greenland Ice Sheet [*Bhatia et al.*, 2013]. In contrast, Antarctic meltwater Fe fluxes are mainly based on a few iceberg measurements [*Hawkings et al.*, 2014], and there are currently no representative data from the Antarctic Ice Sheet (AntIS).

Intense Fe recycling during the weathering of the basal sediment and bedrock material beneath the AntIS may supply nutrients, Fe-rich meltwaters and associated sediments to the Southern Ocean [*Staham et al.*, 2008; *Wadham et al.*, 2010]. These subglacial meltwaters are exported from the AntIS via channels beneath the margins of major ice streams [*Le Brocq et al.*, 2013], which, in turn, terminate in large ice shelves, requiring Fe-enriched subglacial meltwaters to travel great distances before reaching the euphotic waters.

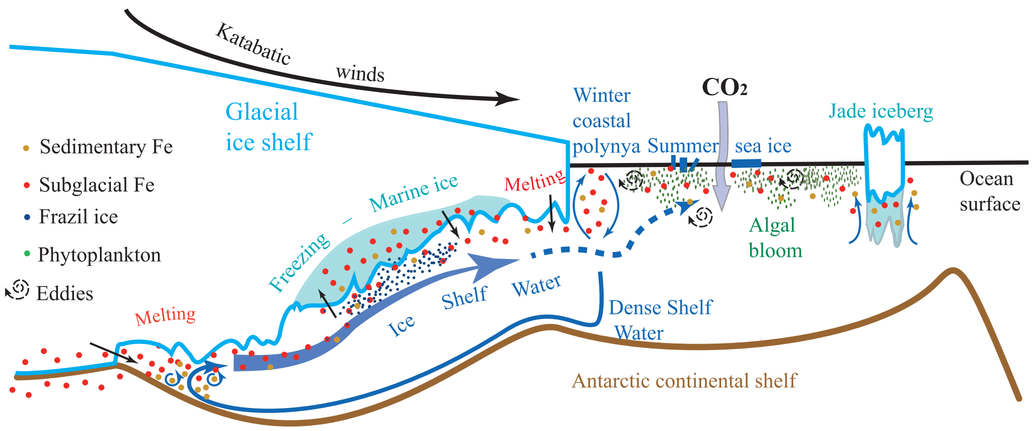

Figure 1. Proposed mechanisms for the delivery of subglacial and sedimentary Fe near grounding lines to the Southern Ocean via marine ice beneath a generalized schematic 2-D section across a cold-regime ice shelf from the grounded ice to the open ocean.

High primary production is observed in these surface waters [e.g., *Smith and Comiso*, 2008]; however, the mechanism for maintaining this productivity remains elusive. Recent research indicates that Fe from Antarctic subglacial sediments may be a key source of Fe for these high productivity ecosystems [*Raiswell et al.*, 2008; *Death et al.*, 2014; *Hawkings et al.*, 2014]. As a result, it has been shown that the Amundsen Sea Polynya is Antarctica's most biologically productive polynya per unit area because of a quasi-continuous supply of meltwater-laden Fe-enriched seawater from the Dotson and Pine Island Glacier ice shelves [*Gerringa et al.*, 2012; *Alderkamp et al.*, 2015; *Sherrell et al.*, 2015]. However, crucial open questions concern (i) the environmental (physical and chemical) processes that transport Fe from beneath the AntIS and ice shelves to the continental shelf waters [*Arrigo et al.*, 2015]; and (ii) the sensitivity of such pathways to current ocean-warming driven increases in ice shelf basal melt and grounding line retreat documented by *Paolo et al.* [2015].

Glacial processes near ice shelf grounding lines are proposed to be particularly vigorous in generating fine lithogenics that release Fe from the subglacial environment to ice shelf cavities and subsequent meltwaters [*Wadham et al.*, 2010]. Under some ice shelves, the interaction between subglacial and ice shelf meltwaters can lead to the formation of a substantial (up to hundreds of meters thick) layer of marine accreted ice. This so-called marine ice layer results from the buoyant accumulation of frazil ice platelets that have formed as a result of supercooling of ice shelf water (Figure 1). The action of the buoyant frazil ice platelets can lead to fine sediment and biogenic material from the ocean being incorporated into the marine ice layer [*Morgan*, 1972; *Warren et al.*, 1983; *Eicken et al.*, 1994; *Roberts et al.*, 2007; *Treverrow et al.*, 2010]. We propose that a marine ice layer accumulates and stores this Fe-rich material, making it an important and previously undocumented Fe-reservoir, delivering subglacial and sedimentary Fe to Antarctic coastal waters.

Here we evaluate the fertilization potential of the marine ice layer beneath the Amery Ice Shelf (AIS) to the observed Chlorophyll-a (Chl-*a*) maximum in Prydz Bay, which is the third most productive bay around Antarctica [*Arrigo and Van Dijken*, 2003]. The bloom in this area has historically comprised primarily diatoms, which can contribute up to 80% of the total cell carbon in Prydz Bay [*Kopczynska et al.*, 1995]. We present (to our knowledge) the first measurements of dissolved and particulate Fe concentrations (hereafter, DFe $< 0.2\ \mu$m and PFe $> 0.2\ \mu$m, respectively) in marine ice from any Antarctic ice shelf; the samples come from an ice core collected in the AIS. We evaluate the fertilization potential of this Fe source to the Fe-deficient Antarctic surface waters. The information on size class (DFe or PFe) allows us to estimate how accessible the Fe is for phytoplankton growth. Dissolved Fe is assumed to be the primary source of Fe available to phytoplankton; however, there is evidence that PFe can become available by leaching dissolved and soluble Fe [*Schroth et al.*, 2009; *Raiswell and Canfield*, 2012].

2. The Amery Ice Shelf and the Formation of the Marine Ice Layer

The AIS fed by the Lambert Glacier system, drains ~16% of the ice area of East Antarctica [*Allison*, 1979] and is the largest ice shelf in the region (~59,000 km^2). As well as being a main drainage route for glacial ice

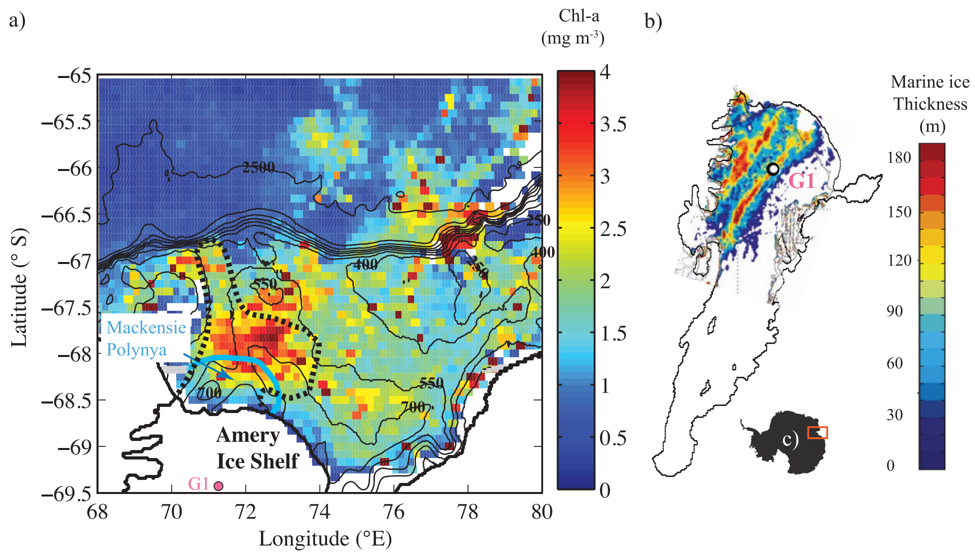

Figure 2. (a) 1997–2010 mean 9 km–SeaWIFS Chlorophyll-a concentration in Prydz Bay. The Chl-*a* mean is for the 8-day composite period from 25 January to 1 February. The black-dashed line shows where the ISW (water mass with temperature below the surface freezing point as a result of ice shelf-ocean interactions) is shallower than 200 m. The area of Mackenzie polynya is outlined in blue. (b) Thickness and distribution of marine ice layer beneath the Amery Ice Shelf [*Fricker et al.*, 2001]. The grounding line is shown in black. (c) Location of the Amery Ice Shelf in East Antarctica.

from the East AntIS, the AIS is potentially a major site for freshwater drainage from beneath the ice sheet. Beneath the AIS, the marine ice layer is up to 190 m thick, accounting for ~ 9% of the ice shelf's volume [*Fricker et al.*, 2001]. This layer is found in the north–western sector of the AIS and extends all the way to the calving front (Figure 2b).

Combined with the local bathymetry, an ice draft of ~2500 m at the southern limit of the AIS grounding zone results in a cavity geometry that supports a strong ice-pump mechanism [*Lewis and Perkins*, 1986]. Within 240 km of the southern limit of the grounding zone, an estimated 80% of the continental ice inflow to the AIS is removed via basal melting [*Craven et al.*, 2009]. The significant freshwater input created by this melting contributes to the formation of bouyant Ice Shelf Water. Ice Shelf Water (ISW) can become supercooled as it rises and flows outward along the shelf cavity slope (because the seawater freezing point increases with depth). In supercooled water, frazil ice platelets accumulate buoyantly on the base of the ice shelf forming a layer of marine accreted ice [e.g., *Oerter et al.*, 1992]. In marine ice samples from the AIS, visible planes and strings of debris in newly accreted marine ice are observed at the elongated linear grain boundaries created by the densification of the frazil ice on the underside of the ice shelf [*Treverrow et al.*, 2010]. This preferential segregation along grain boundaries suggests sediments are incorporated from the water column by the frazil as it rises toward the ice shelf base.

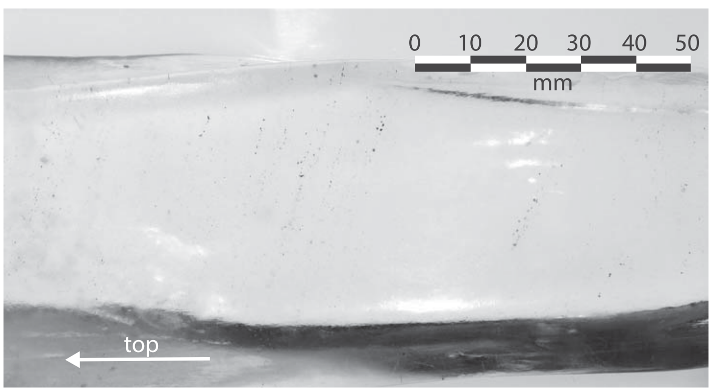

Figure 3. Particulate horizons within a marine ice core retrieved from a depth of 275 m at the AM01 site in 2003. The AM01 borehole has the same geographical location as the G1 site. We analyzed G1 marine ice from a depth of 279 m (Table 1). The vertical (long) axis of core is parallel to the white arrow, which indicates the direction to the ice shelf surface. Note that the core has an irregular (noncircular) cross section, which contributes to the dark appearance of parts the core surface, e.g., along the lower edge of the image.

Sediment strings and layers of 1–2 mm thickness were visible to the naked eye in the G1 site marine ice core used in this study (Figure 3). Similar patterns of particulate inclusions have been observed in marine ice samples recovered more recently from the same geographic location (and elsewhere) on the AIS [*Craven et al.*, 2004; *Treverrow et al.* 2010] and in the J9 marine ice core from the Ronne Ice Shelf [*Eicken et al.*, 1994]. As Fe-bearing sediments must be incorporated into the marine ice layer during accretion, a common process for large-scale marine ice layer formation implies a common process for the inclusion of debris.

The AIS is not the only ice shelf with a marine ice layer. Marine ice layers have also been recorded beneath the Filcher-Ronne, Ross, Hells Gate, Nansen, and southerm McMurdo ice shelves [e.g., *Gow*, 1963; *Zotikov et al.*, 1980; *Souchez et al.*, 1991; *Oerter et al.*, 1992; *Eicken et al.*, 1994; *Tison et al.*, 1998; *Khazendar et al.*, 2001; *Lambrecht et al.*, 2007; *Koch et al.*, 2015], and suggested beneath the West Ice Shelf [*Warren et al.*, 1983]. This list does not preclude marine ice layers in other less studied ice shelves.

3. Materials and Methods

3.1. Samples Location

Samples used for this study were obtained from a 315 m thermally drilled ice core at the G1 site [*Morgan*, 1972] on the AIS (69.44°S, 71.42°E), ~100 km from the shelf front (Figure 2). The marine ice layer at this site is 203 m thick. We analyzed two G1 ice core samples: continental ice from core #102, (of 0.39 m length collected at 254 m depth), and marine ice from core #116 (of 0.44 m length collected at 279 m depth, just below the continental-marine ice transition).

3.2. Laboratory-Based Treatment of the Ice Cores

All plasticware (low-density polyethylene (LDPE) and perfluoroalkoxy (PFA)) used for trace metal work was cleaned as follows: first soaking in a detergent bath (Decon 2% v:v) for 24 h, followed by rinsing 3X with deionized water and then 3X with Ultra High Purity water (UHP) (18.2 MΩ•cm Barnstead water system) before being filled with 6*M* Hydrochloric acid (HCl, Merck, reagent grade) for 1 month. Items were then rinsed 5X with UHP water and dried inside a class-100 laminar flow hood. Bottles and containers were then sealed in triple plastic bags until used. Polycarbonate (PC) filters (0.2 μm porosity, 47 mm diameter, Nuclepore) were treated in 1*M* HCl ultrapure (Seastar Baseline®, Choice Analytical) for 1 week before being gently rinsed 5X and stored in UHP before use. Pipette tips were manipulated inside a class-100 laminar flow hood and rinsed 5X with 6*M* HCl and 5X with UHP before use.

The ice decontamination procedure took place at −10°C, within an ISO class 5 laminar flow bench. The 6–7 cm diameter ice core samples were mounted in a custom-built, polyethylene, hand-driven lathe (on loan from Université Libre de Bruxelles, Belgium). Four 2–3 mm thick annular layers were removed mechanically using a titanium (Ti) cutting blade attached to a ceramic handle [*Lannuzel et al.*, 2006]. The Ti blade is the only lathe component in contact with the ice samples after final sectioning. Ice chips produced during the cleaning procedure of the marine ice core were collected in clean LDPE containers, melted, acidified to pH 1.8 with ultrapure HCl (Seastar Baseline®, Choice Analytical) and analyzed by inductively coupled plasma sector field mass spectrometry (ICP-SF-MS) to verify the effectiveness of the decontamination procedure. Analysis of ice shavings during consecutive decontamination of outer core layers confirmed the efficacy of the decontamination procedure, with a decrease in total dissolvable Fe concentrations between the first (19.8 μ*M*), the second (8.6 μ*M*), third (4.1 μ*M*), and fourth (4.2 μ*M*) layers removed.

For both the continental and marine ice cores, the inner-most cores (3 cm diameter) were cut in half using the lathe to obtain two sections of approximately 10 cm length. Each of the 4 × 10 cm sections was transferred into 1 L wide-mouth LDPE bottles and allowed to melt at ambient temperature before filtration through 0.2 μm PC filter. Filters retaining the particulate material were stored at −30°C in acid-cleaned polystyrene petri dishes until further processing. Total digestion of the filters was performed in 15 mL Teflon® PFA vials (Savillex, Minnetonka, MN, USA) using a mixture of strong acids (0.25 mL 12*M* HCl + 0.25 mL 29*M* HF + 0.5 mL 16*M* HNO_3, all Ultrapure, SeaStar Baseline®, Choice Analytical), dry evaporated for 12 h on a Teflon-coated graphite digestion hot plate housed within a fume extraction cabinet, coupled with HEPA filters to ensure clean input air (all DigiPREP® from SCP Science, France) and resuspended in 10% v:v HNO_3 to dissolve the particulate Fe fraction. The filtered samples were acidified to pH 1.8 using ultrapure HCl (Seastar Baseline®, Choice Analytical) and represent the dissolved fraction.

Table 1. Summary of Dissolved and Particulate Fe Concentrations From Antarctic Sources[a]

Sample Type	DFe (nM)	PFe (nM)
Marine ice 1 (this study)	**339**	**13,323**
Marine ice 2 (this study)	**691**	**14,679**
Continental ice 1 (this study)	**167**	**31**
Continental ice 2 (this study)	**62**	**26**
Antarctic snow in the sea-ice zone [*Lannuzel et al.*, 2010]	0.07–8.45	0.03–3.64
Antarctic pack ice [*Lannuzel et al.*, 2010]	0.23–22.8	0.86–216.71
Iceberg [*Boye et al.*, 2001]	2.8–4.4	
Antarctic iceberg with visible sediments [*Hawkings et al.*, 2014]	0.69 ± 0.87	
Antarctic glaciers with visible sediments [*Hawkings et al.*, 2014]	1.5 ± 1.8	
Law Dome meteoric ice (Total Fe) [*Edwards et al.*, 2006]		0.5–124
Princess Elizabeth Land (mean TDFe) [*Edwards and Sedwick*, 2001]		9–20.8
Antarctic Byrd ice-core (Labile Fe: median concentrations) [*Hiscock et al.*, 2013]	0.59 (preboreal ice)	
	1.51 (glacial ice)	
	2.36 (LGM ice)	
Shelf waters, Southern Ocean compilation (0–100 m, <2000m seafloor depth) [*Tagliabue et al.*, 2012]	0.61 ± 1.14	
Off Shelf waters, Southern Ocean compilation (0–100 m, >2000m seafloor depth) [*Tagliabue et al.*, 2012]	0.38 ± 0.55	
Shelf waters, Amundsen Sea (0–100 m, 0.45–5μm size fraction) [*Planquette et al.*, 2013]		12.1 ± 015.8
Off Shelf waters, Amundsen Sea (0–100 m, 0.45–5 μm size fraction) [*Planquette et al.*, 2013]		0.28 ± 00.29

[a]Concentrations measured in the marine and continental ice cores from the G1 ice core from the Amery Ice Shelf are listed in bold.

3.3. Analytical Methods

The dissolved and particulate Fe fractions were then analyzed by SF-ICP-MS (Thermo Finnigan Element 2) at the University of Tasmania for a suite of key trace elements, following methods described in *Bowie et al.* [2010]. The instrument has three predefined spectral resolutions available enabling isotopes of interest to be quantified with minimal spectral interferences. The SF-ICP-MS was purged by alternating 10% v:v HNO_3, 10% v:v HCl, and UHP water for 2 days prior to sample analysis to ensure low background levels. Indium (In) was added to all samples at a final concentration of 10 μg/L and used as an internal standard. The detection limit is calculated as 3 times the standard deviation of the HNO_3 10% v:v acid blanks (=0.5 n*M*). The samples were handled and introduced to the instrument using an ISO class 5 laminar flow bench.

4. Results and Discussion

4.1. Observed DFe and PFe Concentrations in the AIS Ice Cores

Processes associated with the formation of marine and continental ice differ from each other significantly and it is not surprising that their Fe concentrations and size distribution also differ. The concentrations of DFe (339–691 n*M*) observed in the AIS marine ice samples are up to four orders of magnitude higher than those typical of Southern Ocean surface waters (Table 1), and up to one order of magnitude higher than in the continental ice samples (62–167 n*M*). The DFe concentrations in the continental ice samples are higher than previous estimates from icebergs. Even more striking, the PFe concentration of the marine ice samples (~14,000 n*M*) are three orders of magnitude higher than those in the continental ice (Table 1). Dominance of the PFe phase in the marine ice samples contrasts with the almost even fractionation in the continental ice. Particulate Fe concentrations in AIS continental ice are comparable to levels reported in continental ice at Law Dome (Table 1).

Horizontal sediment layers 1–2 mm thick were visible to the naked eye in the G1 marine ice cores (Figure 3). Microscope observations of the sediment horizons in the AIS marine ice samples suggest that up to 2/3 of the material in these layers is lithogenic [*Roberts et al.*, 2007]. The biogenic component of the marine ice contained mainly sea ice diatoms. As noted in section 2, similar deposits have been observed in other marine ice samples from the Amery [*Craven et al.*, 2004] and Ronne ice shelves [*Eicken et al.*, 1994]. We propose that the presence of subglacial meltwater, with suspended sediments, together with turbulence due to convective and/or melt-driven mixing close to the grounding line [*Jenkins*, 2011] would facilitate the incorporation of DFe and sediments into the ISW. Indeed, suspended sediments are expected to provide solidification nuclei for frazil ice platelet formation in supercooled ISW. This transport mechanism agrees well with the sedimentation regime beneath the Amery, where the overturning circulation (near-bed inflow, surface outflow) has a higher influence on sediment distributions than the depth-integrated circulation (east-inflow, west-outflow) [*Hemer et al.*, 2007]. Additionally, the buoyant accumulation of frazil ice may

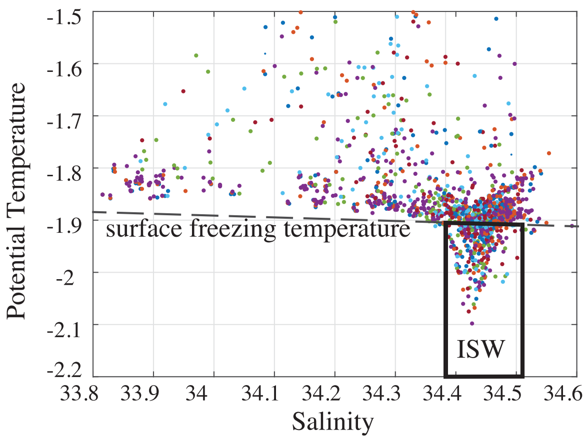

Figure 4. Temperature-Salinity diagram showing the IWS properties in the western flank of Prydz Bay, along the section shown in Figure 5. The colors of the symbols correspond to different seal profiles.

facilitate the scavenging of Fe-rich suspended sediments from shallow water columns and their inclusion within the marine ice layer.

Upper ocean waters may enter the ice shelf cavity and carry Fe into the marine ice layer; however, this input is expected to be low. Warm near-surface waters are able to enter the cavity and cause basal melt up to 100–150 km into the cavity. This inflow will carry both organic matter and open ocean phyto and zooplankton, e.g., *Roberts et al.* [2007]. However, this inflow will cause net melting, rather than formation of marine ice. The lower part of the marine ice layer is permeable, that is, water can circulate within the ice matrix of accreted frazil ice platelets [*Craven et al.*, 2009]. There is a possibility that some DFe and PFe present in this circulating water may be incorporated into the ice matrix. This mechanism would be more efficient in areas of active freezing, where subglacial-sourced Fe presumably dominates than in areas of inflowing surface waters, where there is net melt.

4.2. Origin of the Marine Ice Fe

Other trace metals, such as aluminum (Al), were also analyzed by SF-ICP-MS. The ratios between Fe/Al, Fe/Mn, and Fe/Ti concentrations have the potential to provide information about the source of the measured Fe. In the marine ice, we find Fe/Al ratios of 0.45 ± 0.05 (n = 2). The marine ice therefore has a ratio higher than the Earth's crust (0.33), suggesting an enrichment of Fe occurred relative to Al. Previous studies suggest that elevated Fe/Al ratios are characteristic of glacial/fluvial runoff [*Raiswell et al.*, 2006, 2008; *van der Merwe et al.*, 2015]. Existing data from marine sediments collected directly under the AIS, show an average ratio of 0.28 ± 0.04 (n = 5; A. Post, unpublished data, 2014), which argues against resuspended sediments as the exclusive source of marine ice Fe. Unfortunately, the lack of local data on the possible end-members does not allow us to pin-down which contribution (lithogenic, authigenic, or biogenic) dominates the Fe source.

4.3. ISW Spatial and Temporal Variability

To study the spatial and temporal variability of the ISW plume in front of the AIS, we have used a subset of data from a Southern Indian Ocean database of hydrographic profiles obtained with instrumented Southern elephant seals (*Mirounga leonine*) [*Roquet et al.*, 2014]. ISW is defined here as the water mass with a temperature colder than −1.92°C (we used a slightly colder temperature than the surface freezing point to isolate the ISW plume). ISW spans salinities between 34.38 and 34.53 in Prydz Bay (Figure 4). A map of the minimum depth at which the ISW is observed in the hydrographic profiles, shows ISW in the upper 400 m of the water column between March and May in our data set (Figure 5). As the ISW plume exits the ice shelf cavity, it upwells, reaching the top 50–100 m in the region where the Chl-*a* maxima is observed (Figure 6). Here the stratification is also low, which favors the transfer of Fe from the ISW to the euphotic zone through wind-driven mixing, eddies, and upwelling driven by the melting of icebergs that calved from the western AIS front.

4.4. Impact of AIS Meltwaters on the Local Primary Productivity

The transfer of Fe from the marine ice layer to the ocean can occur via two processes: (i) ice shelf basal melting and (ii) iceberg calving and subsequent melting. High rates of basal melt result from the advection of intermediate shelf waters into ice shelf cavities, primarily by tidal and Ekman currents, topographic edge waves, and ocean eddies [e.g., *Joughin and Padman*, 2003; *Makinson et al.*, 2011]. The AIS marine ice layer extends all the way to the calving front [*Fricker et al.*, 2001] (Figure 2). In the AIS cavity, the ISW infiltrates the unconsolidated part of the marine ice layer [*Herraiz-Borreguero et al.*, 2013], enabling transfer of Fe from the marine ice layer to the ISW.

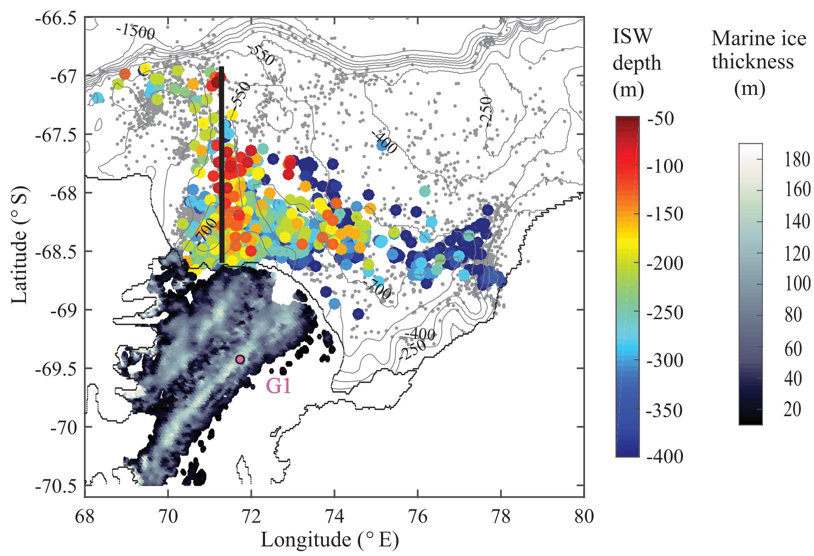

Figure 5. Shallowest depth of ISW between March and April 2011 and 2013. Grey dots are temperature/salinity profiles with no ISW detected. The black vertical line shows the location of the section used to make Figure 5 and 6. The thickness (in meters) of the marine ice layer is also shown on a different color scale. The location of G1 ice core is indicated by a pink circle.

Previous work suggests that about 58% of the variance in mean Chlorophyll concentration in Antarctic polynyas can be explained by basal melting of nearby ice shelves [*Arrigo et al.*, 2015]. Meltwater-laden outflows from Pine Island Glacier and Dotson Ice Shelf cavities are the dominant source of Fe to the Amundsen polynya [*Sherrell et al.*, 2015].

Continental ice icebergs have previously been linked to hot spots of enhanced primary productivity and carbon sequestration [*Raiswell et al.*, 2008]. Icebergs with marine ice are generally referred to as jade

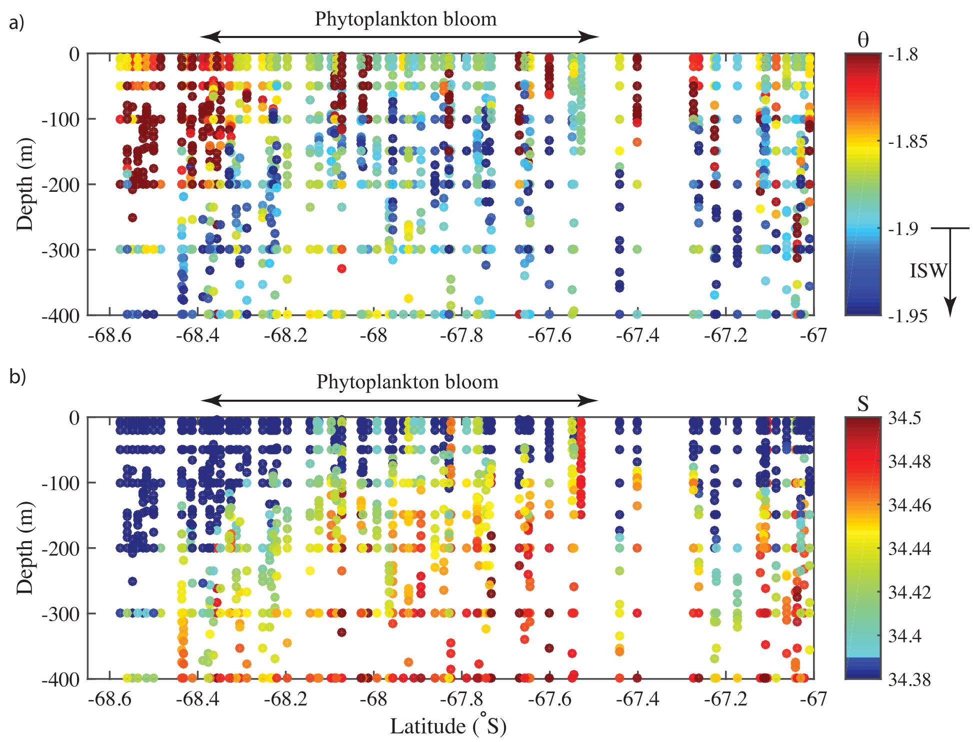

Figure 6. (a) Potential temperature and (b) salinity section across the phytoplankton bloom shown in Figure 2. The section is shown in Figure 4. The profiles used correspond to March 2012–2013.

icebergs. The color of the jade icebergs depends on the color of the water from which the ice formed: if the water contains dissolved organic matter (yellow or brown), then some of it gets incorporated into the ice and the ice appears green (S. Warren, personal communication, 2013). But not all marine ice is green; it can also be dark blue and yellow-green [*Warren et al.*, 1997]. Jade-coloured icebergs are commonly observed near the AIS and exported out of Prydz Bay and their role in Fe fertilization has not previously been assessed.

Several processes can explain the delivery of Fe to the observed phytoplankton bloom. Beneath the ice shelf, the lower layer of the marine ice is unconsolidated and porous [*Craven et al.*, 2004] allowing seawater to flow through it and immediately below it [*Herraiz-Borreguero et al.*, 2013], likely transferring PFe and DFe from the marine ice to ISW and upper waters in regions where basal melting occurs. The low salinity of the marine ice ($S < 1$) [*Craven et al.*, 2004] gives additional buoyancy to the marine ice meltwater and seawater mixture. The satellite-derived Chl-*a* maximum lies within the primary export path of both the ISW and the sediment-rich jade icebergs (Figures 2a and 5). Outside the ice shelf cavity, winter deep convection in the Mackenzie polynya is expected to transport the Fe-bearing (and other nutrients) ISW to the surface (Figure 1) where it will become available for phytoplankton early in the austral summer. However, this Fe is likely consumed very fast and may not be enough to sustain the bloom (Figure 2a) [*Alderkamp et al.*, 2015]. In summer, the ISW plume shallows as it moves northward from the ice shelf front, reaching a minimum depth of ~50 m within the bloom area (Figure 4a). Frazil ice suspended within supercooled ISW has also been observed outside the ice shelf cavity during the summer and winter [*Penrose et al.*, 1994]. The upwelling of frazil ice is likely to favor the transport of Fe to the euphotic zone. Isohalines shoal in this area (Figure 6), suggesting the upper water column is less stratified than surrounding waters, allowing wind-driven mixing and mesoscale eddies to upwell Fe to the euphotic zone where it is accessible to phytoplankton. In addition, the melting of jade icebergs calved from the AIS creates local upwelling that will also contribute to carry Fe up to the euphotic zone (Figure 1). The AIS is a major source of large icebergs [*Smith et al.*, 2013], which are able to enhance Chlorophyll significantly as early as 6 days after the passing of an iceberg, and by a factor of ten a month or more later [*Duprat et al.* 2016]. Iron concentrations in jade icebergs can be orders of magnitude higher than in continental ice, so it is reasonable to expect jade icebergs to increase marine productivity locally. These processes are shown schematically in Figure 1.

4.4.1. Iron Supply From the AIS

Within the marine ice layer of the Ronne Ice Shelf, horizons of sediments are 0.3 to 1.2 mm thick and separated from one another by a few millimeters [*Eicken et al.*, 1994]. Given the common processes governing sediment inclusions during marine ice formation in both the Ronne and Amery ice shelves, it is expected that this type of sediment layering is similarly prevalent in the AIS. The narrow spacing of the sediment horizons suggests that Fe is evenly distributed within the marine ice layer. Consequently, we use the mean DFe concentration (515 n*M*) from Table 1 to calculate the potential Fe flux from the marine ice layer.

The proportion of marine ice in the calving zone of the Amery Ice Shelf (estimated as the region within ~50 km of the shelf front) was calculated using marine ice thickness [*Fricker et al.*, 2001] and total ice shelf thickness [*Fretwell et al.*, 2013] data sets. Marine ice represents ~13% of the total ice shelf volume at the calving front and the marine ice calving flux is concentrated in the western half of the ice shelf where the marine ice layer is observed. Iceberg calving is responsible for ~60% of the total AIS mass loss or a calving flux of 50 ± 6 Gt/yr [*Depoorter et al.* 2013]. If we conservatively assume that half of the calving front contains marine ice, then we have a marine ice calving flux of 3.25 ± 2.43 Gt/yr. Using the mean DFe concentration of marine ice (515 n*M*) and the calculated calving flux of marine ice (3.25 ± 2.43 Gt/yr), we calculate the portion of the total AIS marine ice DFe flux that is delivered by calving of jade icebergs as 0.09 ± 0.07 Gg/yr of DFe.

To estimate the total AIS Fe flux into Prydz Bay released by marine ice through basal melting and iceberg calving, we use the mean DFe concentration (515 n*M*) from Table 1. We then consider a steady state between the rate of marine ice accretion and the rates of marine ice melting and calving. Estimates of the mean marine ice accretion rate beneath the AIS range from 5–16 Gt/yr [*Wen et al.,* 2010; *Galton-Fenzi et al.*, 2012], resulting in a DFe flux due to marine ice basal melt of 0.14–0.46 Gg/yr into Prydz Bay. Assuming that 0.15% (Fe ascorbate solubility of glacial meltwater and iceberg-AntIS, from *Hawkings et al.* [2014] and *Raiswell et al.* [2010]) of the PFe (21 n*M*) becomes bioavailable, we obtain an additional Fe flux of 0.01–0.02 Gg/yr, giving a total assumed-bioavailable Fe flux from marine ice calving and basal melt of 0.15–0.48 Gg/yr.

Since we measured DFe and PFe concentrations in continental ice (means of 114.5 and 28.9 n*M*, respectively; Table 1), we can also estimate the potential flux of assumed bioavailable Fe released from continental ice into Prydz Bay via basal melt and iceberg calving. Continental ice basal melting rate from the AIS is estimated at 46 $\pm$ 6.9 Gt/yr [*Wen et al.*, 2010; *Galton-Fenzi et al.*, 2012], resulting in a DFe flux due to continental ice calving and basal melt of 0.30 $\pm$ 0.04 Gg/yr into Prydz Bay. The fraction of potentially bioavailable PFe in continental ice is low (0.04 n*M*) compared to marine ice, leading to a negligible additional bioavailable Fe flux of 1.1 $\times$ 10^{-4} Gg/yr. Note that these fluxes are conservative as: we assume: (i) a constant melt rate throughout the year (in reality we would expect higher melt rates during the austral summer when seasonally warmer upper ocean waters just north of the ice front occur, and the Chl-*a* maximum develops in western Prydz Bay); and, (ii) a very low PFe solubility of 0.15%, compared with estimates up to 30% for dust [*Edwards and Sedwick*, 2001] and 40% for suspended particles (*van der Merwe*, 2015).

Overall, the total assumed bioavailable Fe flux contributions of marine and continental ice from the AIS are similar (i.e., 0.15–0.48 Gg/yr versus 0.30 $\pm$ 0.04 Gg/yr, respectively). Previous studies have highlighted the role of continental ice as a source of Fe to Antarctic surface waters either via glacial melt [*Raiswell et al.*, 2006; *Gerringa et al.*, 2012] or floating icebergs [*Raiswell et al.,* 2008; *Lin et al.,* 2011; *Raiswell*, 2011; *Shaw et al.*, 2011]. Our study is the first to demonstrate that marine ice equals continental ice in the supply of bioavailable Fe to surface waters in the AIS region. The storage capacity of Fe within the marine ice layer and the expected higher melt rates in summer make the marine ice a more effective source of Fe to the phytoplankton.

4.4.2. Iron Demand in the Bloom Area

Phytoplankton biomass in the upper mixed layer was approximated by measurements of the 1997–2010 average SeaWIFS satellite derived (8 day composite image, 9 $\times$ 9 km grid) Chl-*a* concentration in the western Prydz Bay during the November–March season ($\sim$2 mg Chl-*a* m^{-3}; Figure 1). The 8 day composite corresponds to 25 January to 1 February. For the biomass calculation, we used the phytoplankton C: Chl-*a* ratio (100 $g.g^{-1}$) [*Thompson et al.*, 1992], an area of 1.7 $\times$ 10^{10} m^2 ($-$67.05 to $-$68.5°S; 71.18–73.75°E) and 100 m upper mixed layer. Our estimate of 100 m is based on the seal data, which shows summer mixed layers ranging from 40 to 150 m deep. This gives an average biomass of 0.34 $\times$ 10^{12} g C over the 1997–2010 November–March season. We find that an Fe flux of 0.03 μmol/m^2/d is required to sustain this bloom when using an averaged cellular Fe:C of 12 μmol/mol [*Hassler and Schoemann*, 2009] and a growth rate for diatoms species of 1.5 d^{-1} [*Sarthou et al.*, 2005]. To calculate our flux of assumed-bioavailable Fe (DFe + 0.15%PFe) delivered from the AIS to the bloom area, we used 0.15–0.48 Gg Fe/yr from marine ice and 0.30 $\pm$ 0.04 Gg Fe/yr from continental ice, a water volume of 8.5 $\times$ 10^{12} m^3 ($-$67.05 to $-$68.5°S; 71.18–73.75°E, 500 deep) and a 100 m upper mixed layer. Note that in this calculation, we are assuming that the Fe released from the AIS will be diluted throughout the 500 m water column, while the phytoplankton will only have access to the Fe within the upper 100 m. The assumed bioavailable Fe flux from continental (0.17 $\pm$ 0.02 μmol/m^2/d) and marine ice (0.09–0.28 μmol/m^2/d) released in the vicinity of the AIS bloom is about an order of magnitude larger than the amount of Fe required to sustain the observed Chl-*a* concentrations (0.03 μmol/m^2/d).

While a fraction of the Fe released from the AIS will be lost to precipitation, scavenging, and potentially supplied to deeper waters below the euphotic zone, our calculations show that only around 7–12% of the total Fe flux from the AIS is necessary to sustain the observed bloom. Even though our flux estimates are limited by the data available, it is apparent that AIS-derived Fe has the potential to start and sustain the observed primary productivity in Prydz Bay. Furthermore, the jade icebergs calved from the AIS that do not melt in the vicinity of the bloom area will transport bioavailable Fe into HNLC waters off the shelf break with even lower ambient DFe concentrations, driving further phytoplankton production. Although the fertilization potential of marine ice is clear, other factors could collectively contribute to the high Chl-*a* in the AIS area during the growing season such as the width of the continental shelf, the sea surface temperature, and area of open waters.

More measurements are needed to quantify all the Fe sources and physical processes responsible for the onset and duration of the phytoplankton bloom in Prydz Bay. Our finding of high concentrations of Fe in AIS marine ice and recent data on increasing rates of ice shelf basal melt in many of Antarctica's ice shelves [*Paolo et al.*, 2015] should motivate further research into the distribution and solubility of Fe in Antarctic marine and continental ice, and the implications of increasing rates of ice shelf basal melt on the marine productivity in Antarctica waters.

5. Conclusions

We have reported the first Fe concentration measurements on marine ice from an Antarctic ice shelf. The data point to a key role for marine ice as a reservoir and transport pathway for subglacial and/or sediment-derived Fe to continental shelf waters; linking the subglacial environment and the marine ecosystem. We also find that the Fe flux contribution of marine ice equals (and most likely exceeds, since we used a very conservative 0.15% PFe solubility estimate) that of continental ice. Changes under ice shelves and near the grounding lines are now recognized as being potentially rapid in response to ocean warming [*Paolo et al.*, 2015]. How ocean warming will affect the formation and thickness of existing marine ice layers is currently unknown, however there is evidence that the marine ice layers beneath the Ross and Ronne ice shelves are thinning [*Paolo et al.,* 2015]. Previous work has shown that the variance in Chl-*a* concentrations in Antarctic coastal polynyas is highly correlated with net ice shelf basal melt rates [*Arrigo et al.*, 2015]. Here we have identified a new mechanism: marine ice iron storage and release, by which basal melt may stimulate such productivity. Our results underline the importance of (i) improving constraints on the distribution, volume and Fe concentration in marine ice beneath Antarctic ice shelves and (ii) understanding how glacial and marine sediment transport will be affected by increasing basal melting. In our view, future work in these areas would help improve understanding of the sources of variability in Antarctic coastal primary productivity and the ability of this region to sequester atmospheric CO_2.

Acknowledgments
This research was supported by the Australian Research Council grant DE120100030 and the Australian Government Cooperative Research Centres Programme through the Antarctic Climate & Ecosystems (ACE CRC). We thank the Australian Antarctic Division for allowing us to use the AIS marine and continental ice cores and Mike Craven for his assistance in the freezer. Elephant seals data are found in the following link: http://dx.doi.org/10/srk). We are also grateful to Ashley Townsend for assistance with the SF-ICP-MS analyses, to Jean–Louis Tison for lending us the lathe and chisels to perform the decontamination of the ice cores, and to Alix Post for sharing her trace metal measurements in the sediment cores within the AIS cavity. We also thank two anonymous reviewers, whose thorough reviews have greatly improved this manuscript.

References

Alderkamp, A.-C., et al. (2012), Iron from melting glaciers fuels phytoplankton blooms in Amundsen Sea (Southern Ocean); Phytoplankton characteristics and productivity, *Deep Sea Res., Part II*, *71–76*, 32–48, doi:10.1016/j.dsr2.2012.03.005.

Alderkamp, A. C., et al. (2015), Fe availability drives phytoplankton photosynthesis rates during spring bloom in the Amundsen Sea Polynya, Antarctica, *Elementa*, *3*(1), 43 pp., doi:10.12952/journal.elementa.000043.

Allison, I. (1979), The mass budget of the Lambert Glacier drainage basin, Antarctica, *J. Glaciol.*, *22*(87), 223–235.

Arrigo, K. R., and G. L. Van Dijken (2003), Phytoplankton dynamics within 37 Antarctic coastal polynya systems, *J. Geophys. Res.*, *108*(C8), 3271, doi:10.1029/2002JC001739.

Arrigo, K. R., G. L. van Dijken, and A. L. Strong (2015), Environmental controls of marine productivity hot spots around Antarctica, *J. Geophys. Res. Oceans*, *120*, 5545–5565, doi:10.1002/2015JC010888.

Bhatia, M. P., E. B. Kujawinski, S. B. Das, C. F. Breier, P. B. Henderson and M. A. Charette (2013), Greenland meltwater as a significant and potentially bioavailable source of iron to the ocean, *Nat. Geosci.*, *6*(4), 274–278.

Bowie, A. R., A. T. Townsend, D. Lannuzel, T. A Remenyi, and P. van der Merwe (2010), Modern sampling and analytical methods for the determination of trace elements in marine particulate material using magnetic sector inductively coupled plasma-mass spectrometry, *Anal. Chim. Acta*, *676*(1-2), 15–27, doi:10.1016/j.aca.2010.07.037.

Boye, M., C. M. G. van den Berg, J. de Jong, H. Leach, P. Croot, and H. J. W. de Baar (2001), Organic complexation of iron in the Southern Ocean, *Deep Sea Res., Part I*, *48*(6), 1477–1497, doi:10.1016/S0967-0637(00)00099-6.

Craven, M., I. Allison, R. Brand, A. Elcheikh, J. Hunter, M. Hemer, and S. Donoghue (2004), Initial borehole results from the Amery Ice Shelf hot-water drilling project, *Ann. Glaciol.*, *39*(1), 531–539, doi:10.3189/172756404781814311.

Craven, M., I. Allison, H. A. Fricker and R. Warner (2009), Properties of a marine ice layer under the Amery Ice Shelf, *J. Glaciol.*, *55*(192), 717–728.

Death, R., J. L. Wadham, F. Monteiro, A. M. Le Brocq, M. Tranter, A. Ridgwell, S. Dutkiewicz, and R. Raiswell (2014), Antarctic ice sheet fertilises the Southern Ocean, *Biogeosciences*, *11*(10), 2635–2643, doi:10.5194/bg-11-2635-2014.

de Baar, H. J., A. Buma, R. F. Nolting, G. C. Cadee, G. Jacques, and P. J. Treguer (1990), On iron limitation of the Southern Ocean: Experimental observations in the Weddell and Scotia Seas, *Mar. Ecol. Prog. Ser.*, *65*, 105–122, doi:10.3354/meps065105.

Depoorter, M. A, J. L. Bamber, J. A. Griggs, J. T. M. Lenaerts, S. R. M. Ligtenberg, M. R. van den Broeke, and G. Moholdt (2013), Calving fluxes and basal melt rates of Antarctic ice shelves, *Nature*, *502*(7469), 89–92, doi:10.1038/nature12567.

Duprat, L. P., G. R. Bigg, and D. J. Wilton (2016), Enhanced southern ocean marine productivity due to fertilization by giant icebergs, *Nat. Geosci.*, *9*, 219–221, doi:10.1038/NGEO2633.

Edwards, R., and P. Sedwick (2001), Iron in East Antarctic snow: Implications for atmospheric iron deposition and algal production in Antarctic waters, *Geophys. Res. Lett.*, *28*(20), 3907–3910, doi:10.1029/2001GL012867.

Edwards, R., P. Sedwick, V. Morgan, and C. Boutron (2006), Iron in ice cores from Law Dome: A record of atmospheric iron deposition for maritime East Antarctica during the Holocene and Last Glacial Maximum, *Geochem. Geophys. Geosyst.*, *7*, Q12Q01, doi:10.1029/2006GC001307.

Eicken, H., H. Oerter, H. Miller, W. Graf, and J. Kipfstuhl (1994), Textural characteristics and impurity content of meteoric and marine ice in the Ronne Ice Shelf, Antarctica, *J. Glaciol.*, *40*(135), 386–398.

Fan, S. M., W. J. Moxim, and H. Levy (2006), Aeolian input of bioavailable iron to the ocean, *Geophys. Res. Lett.*, *33*, L07602, doi:10.1029/2005GL024852.

Fretwell, P., et al. (2013), Bedmap2: Improved ice bed, surface and thickness datasets for Antarctica, *Cryosphere*, *7*(1), 375–393, doi:10.5194/tc-7-375-2013.

Fricker, H. A., S. V. Popov, I. Allison, and N. W. Young (2001), Distribution of marine ice beneath the Amery Ice Shelf, *Geophys. Res. Lett.*, *28*(11), 2241–2244.

Galton-Fenzi, B. K., J. R. Hunter, R. Coleman, S. J. Marsland, and R. C. Warner (2012), Modeling the basal melting and marine ice accretion of the Amery Ice Shelf, *J. Geophys. Res.*, *117*, C09031, doi:10.1029/2012JC008214.

Gerringa, L. J. A., A. Alderkamp, P. Laan, C. Thuroczy, H. J. W. de Baar, M. M. Mills, G. L. Van Dijken, H. Van Haren, and K. R. Arrigo (2012), Iron from melting glaciers fuels the phytoplankton blooms in Amundsen Sea (Southern Ocean): Iron biogeochemistry, *Deep Sea Res., Part I*, *71–76*, 16–31.

Gow, A. (1963), The inner structure of the Ross Ice Shelf at Little America, Antarctica, as revealed by deep core drilling, in *IUGG General Assembly of Berkeley, Int. Assoc. Sci. Hydrol. Publ.*, *61*, 272–284.

Hawkings, J. R., J. L. Wadham, M. Tranter, R. Raiswell, L. G. Benning, P. J. Statham, A. Tedstone, P. Nienow, K. Lee, and J. Telling (2014), Ice sheets as a significant source of highly reactive nanoparticulate iron to the oceans, *Nat. Commun.*, *5*, 3929, doi:10.1038/ncomms4929.

Hassler, C. S., and V. Schoemann (2009), Bioavailability of organically bound Fe to model phytoplankton of the Southern Ocean, *Biogeosci. Discussion*, *6*, 1677–1712.

Hemer, M. A., A. L. Post, P. E. O'Brien, M. Craven, E. M. Truswell, D. Roberts, and P. T. Harris (2007), Sedimentological signatures of the sub-Amery Ice Shelf circulation, *Antarct. Sci.*, *19*(4), 497–506, doi:10.1017/S0954102007000697.

Herraiz-Borreguero, L., I. Allison, M. Craven, K. W. Nicholls, and M. A. Rosenberg (2013), Ice shelf/ocean interactions under the Amery Ice Shelf: Seasonal variability and its effect on marine ice formation, *J. Geophys. Res. Oceans*, *118*, 7117–7131, doi:10.1002/2013JC009158.

Hiscock, W. T., H. Fischer, M. Bigler, G. Gfeller, and D. Leuenberger (2013), Continuous flow analysis of labile iron in ice-cores, *Environ. Sci. Technol.*, *47*, 4416–4425.

Jenkins, A. (2011), Convection-driven melting near the grounding lines of ice shelves and tidewater glaciers, *J. Phys. Oceanogr.*, *41*(12), 2279–2294, doi:10.1175/JPO-D-11-03.1.

Jickells, T. D., et al. (2005), Global iron connections between desert dust, ocean biogeochemistry, and climate, *Science*, *308*, 67–73.

Joughin, I., and L. Padman (2003), Melting and freezing beneath Filchner-Ronne ice shelf, Antarctica, *Geophys. Res. Lett.*, *30*(9), 1477, doi:10.1029/2003GL016941.

Khazendar, A., J. L. Tison, B. Stenni, M. Dini, and A. Bondesan (2001), Significant marine ice accumulation in the ablation zone beneath an Antarctic ice shelf, *J. Glaciol.*, *47*, 359–368, doi:10.3189/172756501781832160.

Koch, I., S. Fitzsimons, D. Samyn, and J.-L. Tison (2015), Marine ice recycling at the southern McMurdo Ice Shelf, Antarctica, *J. Glaciol.*, *61*(228), 689–701, doi:10.3189/2015JoG14J095.

Kopczynska, E., L. Goeyens, M. Semeneh, and F. Dehairs (1995), Phytoplankton composition and cell carbon distribution in Prydz Bay, Antarctica: Relation to organic particulate matter and its delta-13C values, *J. Plankton Res.*, *17*(4), 685–707, doi:10.1093/plankt/17.4.685.

Lambrecht, A., H. Sandhäger, D. Vaughan, and C. Mayer (2007), New ice thickness maps of Filchner-Ronne Ice Shelf, Antarctica, with specific focus on grounding lines and marine ice, *Antarct. Sci.*, *19*(4), 507–519.

Lannuzel, D., J. de Jong, V. Schoemann, A. Trevena, J.-L. Tison, and L. Chou (2006), Development of a sampling and flow injection analysis technique for iron determination in the sea ice environment, *Anal. Chim. Acta*, *556*(2), 476–483, doi:10.1016/j.aca.2005.09.059.

Lannuzel, D., V. Schoemann, J. De Jong, J. L. Tison, and L. Chou (2007), Distribution and biogeochemical behaviour of iron in the East Antarctic sea ice, *Mar. Chem.*, *106*(1), 18–32.

Lannuzel, D., V. Schoemann, J. de Jong, B. Pasquer, P. van der Merwe, F. Masson, J.-L. Tison, and A. Bowie (2010), Distribution of dissolved iron in Antarctic sea ice: Spatial, seasonal, and inter-annual variability, *J. Geophys. Res.*, *115*, G03022, doi:10.1029/2009JG001031.

Le Brocq, A. M, et al. (2013), Evidence from ice shelves for channelized meltwater flow beneath the Antarctic Ice Sheet, *Nat. Geosci.*, *6*(11), 945–948, doi:10.1038/ngeo1977.

Lewis, E., and R. Perkins (1986), Ice pumps and their rates, *J. Geophys. Res.*, *91*(C10), 11,756–11,762.

Lin, H., S. Rauschenberg, C. R. Hexel, T. J. Shaw, and B. S. Twining (2011), Free-drifting icebergs as sources of iron to the Weddell Sea, *Deep Sea Res., Part II*, *58*(11–12), 1392–1406, doi:10.1016/j.dsr2.2010.11.020.

Makinson, K., P. R. Holland, A. Jenkins, K. W. Nicholls and D. M. Holland (2011), Influence of tides on melting and freezing beneath Filchner-Ronne Ice Shelf, Antarctica, *Geophys. Res. Lett.*, *38*, L06601, doi:10.1029/2010GL046462.

Morgan, V. (1972), Oxygen isotope evidence for bottom freezing on the Amery Ice Shelf, *Nature*, *238*, 393–394, doi:10.1038/238393a0.

Oerter, H., J. Kipfstuhl, J. Determann, H. Miller, D. Wagenbach, A. Minikin, and W. Graf (1992), Evidence for basal marine ice in the Filchner-Ronne ice shelf, *Nature*, *358*(6385), 399–401.

Paolo, F. S., H. A. Fricker, and L. Padman (2015), Volume loss from Antarctic ice shelves is accelerating, *Science*, *348*(80), 327–331.

Penrose, J. D., M. Conde, and T. J. Pauly (1994), Acoustic detection of ice crystals in Antarctic waters, *J. Geophys. Res.*, *99*(C6), 12,373–12,380.

Planquette, H., R. M. Sherrell, S. Stammerjohn, and P. M. Field (2013), Particulate iron delivery[10.1016/j.marchem.2013.04.006] to the water column of the Amundsen Sea, Antarctica, *Mar. Chem.*, *153*, 15–30, doi:10.1016/j.marchem.2013.04.006.

Raiswell, R., H. P. Vu, L. Brinza, and L.G. Benning (2009), The determination of labile Fe in ferrihydrite by ascorbic acid extraction: Methodology, dissolution kinetics and loss of solubility with age and de-watering, *Chemical Geology*, *278*(1-2), 70–79, doi:10.1016/j.chemgeo.2010.09.002.

Raiswell, R. (2011), Iceberg-hosted nanoparticulate Fe in the Southern Ocean: Mineralogy, origin, dissolution kinetics and source of bioavailable Fe, *Deep Sea Res., Part II*, *58*(11–12), 1364–1375.

Raiswell, R., and D. E. Canfield (2012), The iron biogeochemical cycle past and present, *Geochem. Perspect.*, *1*(1), 1–220, doi:10.7185/geochempersp.1.1.

Raiswell, R., M. Tranter, L. G. Benning, M. Siegert, R. Death, P. Huybrechts, and T. Payne (2006), Contributions from glacially derived sediment to the global iron (oxyhydr)oxide cycle: Implications for iron delivery to the oceans, *Geochim. Cosmochim. Acta*, *70*(11), 2765–2780, doi:10.1016/j.gca.2005.12.027.

Raiswell, R., L. G. Benning, M. Tranter, and S. Tulaczyk (2008), Bioavailable iron in the Southern Ocean: The significance of the iceberg conveyor belt, *Geochem. Trans.*, *9*, 1–9, doi:10.1186/1467-4866-9-7.

Roberts, D., M. Craven, M. Cai, I. Allison, and G. Nash (2007), Protists in the marine ice of the Amery Ice Shelf, East Antarctica, *Polar Biol.*, *30*(2), 143–153, doi:10.1007/s00300-006-0169-7.

Roquet, F., et al. (2014), A Southern Indian Ocean database of hydrographic profiles obtained with instrumented elephant seals, *Sci. Data*, *1*, 140028, doi:10.1038/sdata.2014.28.

Sarthou, G., K. R. Timmermans, S. Blain, and P. Tréguer (2005), Growth physiology and fate of diatoms in the ocean: A review, *J. Sea Res.*, *53*(1–2), 25–42, doi:10.1016/j.seares.2004.01.007.

Schroth, A. W., J. Crusius, E. R. Sholkovitz, and B. C. Bostick (2009), Iron solubility driven by speciation in dust sources to the ocean, *Nat. Geosci.*, *2*, 337–340, doi:10.1038/NGEO501.

Shaw, T. J., R. Raiswell, C. R. Hexel, H. P. Vu, W. S. Moore, R. Dudgeon, and K. L. Smith (2011), Input, composition and potential impact of terrigenous material from free-drifting icebergs, *Deep Sea Res., Part II*, *58*, 1376–1383.

Sherrell, R. M., M. E. Lagerström, K. O. Forsch, S. E. Stammerjohn, and P. L. Yager (2015), Dynamics of dissolved iron and other bioactive trace metals (Mn, Ni, Cu, Zn) in the Amundsen Sea Polynya, Antarctica, *Elementa*, *3*(1), 71 pp., doi:10.12952/journal.elementa.000071.

Smith, K. L., A. D. Sherman, T. J. Shaw, A. E. Murray, M. Vernet, and A. O. Cefarelli (2011), Carbon export associated with free-drifting icebergs in the Southern Ocean, *Deep Sea Res., Part II*, *58*, 1485–1496.
Smith K. L., Jr., A. D. Sherman, T. J. Shaw and J. Sprintall (2013), Icebergs as unique Lagrangian ecosystems in polar seas, *Annu. Rev. Mar. Sci.*, *5*, 269–287, doi:10.1146/annurev-marine-121211-172317.
Smith, W. O., and J. C. Comiso (2008), Influence of sea ice on primary production in the Southern Ocean: A satellite perspective, *J. Geophys. Res.*, *113*, C05S93, doi:10.1029/2007JC004251.
Staham, P. J., M. Skidmore, and M. Tranter (2008), Inputs of glacially derived dissolved and colloidal iron to the coastal ocean and implications for primary productivity, *Global Biogeochem. Cycles*, *22*, GB3013, doi:10.1029/2007GB003106.
Souchez, R., M. Meneghel, J.-L. Tison, R. Lorrain, D. Ronveaux, C. Baroni, A. Lozej, I. Tabacco, and J. Jouzel (1991), Ice composition evidence of marine ice transfer along the bottom of a small Antarctic ice shelf, *Geophys. Res. Lett.*, *18*(5), 849–852.
Tagliabue, A., T. Mtshali, O. Aumont, A. R. Bowie, M. B. Klunder, A. N. Roychoudhury and S. Swart (2012), A global compilation of dissolved iron measurements: Focus on distributions and processes in the Southern Ocean. *Biogeosciences*, *9*(6), 2333–2349.
Tagliabue, A., J. B. Sallée, A. R. Bowie, M. Lévy, S. Swart, and P. W. Boyd (2014), Surface-water iron supplies in the Southern Ocean sustained by deep winter mixing, *Nat. Geosci.*, *7*, 314–320, doi:10.1038/ngeo2101.
Thompson, P. A., M. Guo, and P. J. Harrison (1992), Effect of variation in temperature. I. On the biochemical composition of eight species of marine phytoplankton, *J. Phycol.*, *28*, 481–488.
Tison, J.-L., R. Lorrain, A. Bouzette, M. Dini, A. Bondesan, and M. Stiévenard (1998), Linking landfast sea ice variability to marine ice accretion at the Hells Gate Ice Shelf, Ross Sea, in *Antarctic Research Series, Antarctic Sea Ice: Physical Processes, Interactions and Variability*, vol. 74, edited by M. Jeffries, pp. 375–407, AGU, Washington, D. C.
Treverrow, A., R. C. Warner, W. F. Budd, and M. Craven (2010), Meteoric and marine ice crystal orientation fabrics from the Amery Ice Shelf, East Antarctica, *J. Glaciol.*, *56*(199), 877–890.
van der Merwe, P., D. Lannuzel, C. Mancuso Nichols, K. Meiners, P. Heil, L. Norman, D. N. Thomas, A. Bowie (2009), Biogeochemical observations during the winter–spring transition in East Antarctic sea ice: Evidence of iron and exopolysaccharide controls, *Mar. Chem.*, *115*, 163–175.
van der Merwe, P., et al. (2015), Sourcing the iron in the naturally fertilised bloom around the Kerguelen Plateau: Particulate trace metal dynamics, *Biogeosciences*, *12*, 739–755.
Wadham, J. L., M. Tranter, M. Skidmore, A. J. Hodson, J. Priscu, W. B. Lyons, M. Sharp, P. Wynn, and M. Jackson (2010), Biogeochemical weathering under ice: Size matters, *Global Biogeochem. Cycles*, *24*, GB3025, doi:10.1029/2009GB003688.
Warren, S. G., C. S. Roesler, V. I. Morgan, R. E. Brandt, I. D. Goodwin, and I. Allison (1983), Green icebergs formed by freezing of organic-rich seawater to the base of Antarctic Ice shelves, *J. Geophys. Res.*, *98*(C4), 6921–6928.
Warren, S. G., C. S. Roesler and R. E. Brandt (1997), Solar radiation processes in the east Antarctic sea-ice zone, *Antarct. J.*, *32*, 185–187.
Wen, J., Y. Wang, W. Wang, K. C. Jezek, H. Liu, and I. Allison (2010), Basal melting and freezing under the Amery Ice Shelf, East Antarctica, *J. Glaciol.*, *56*(195), 81–90, doi:10.3189/002214310791190820.